



**HAL**  
open science

# Three-dimensional numerical simulation of droplet formation by Rayleigh–Taylor instability in multiphase corium

R. Zanella, R. Le Tellier, M. Plapp, G. Tegze, H. Henry

► **To cite this version:**

R. Zanella, R. Le Tellier, M. Plapp, G. Tegze, H. Henry. Three-dimensional numerical simulation of droplet formation by Rayleigh–Taylor instability in multiphase corium. Nuclear Engineering and Design, 2021, 379, pp.111177. 10.1016/j.nucengdes.2021.111177. hal-03383161

**HAL Id: hal-03383161**

**<https://hal.science/hal-03383161>**

Submitted on 18 Oct 2021

**HAL** is a multi-disciplinary open access archive for the deposit and dissemination of scientific research documents, whether they are published or not. The documents may come from teaching and research institutions in France or abroad, or from public or private research centers.

L'archive ouverte pluridisciplinaire **HAL**, est destinée au dépôt et à la diffusion de documents scientifiques de niveau recherche, publiés ou non, émanant des établissements d'enseignement et de recherche français ou étrangers, des laboratoires publics ou privés.

# Three-dimensional numerical simulation of droplet formation by Rayleigh-Taylor instability in multiphase corium

R. Zanella<sup>1</sup>, G. Tegze<sup>2</sup>, M. Plapp<sup>1</sup>, R. Le Tellier<sup>3</sup>, and H. Henry<sup>1</sup>

<sup>1</sup>Laboratoire PMC, Ecole Polytechnique, CNRS, IP Paris, 91128 Palaiseau Cedex, France,  
zanella.raphael@gmail.com, herve.henry@polytechnique.edu,  
mathis.plapp@polytechnique.edu

<sup>2</sup>Wigner Research Centre for Physics, P.O. Box 49, H-1525 Budapest, Hungary,  
tegze.gyorgy@wigner.mta.hu

<sup>3</sup>CEA, DES, IRESNE, DTN, Cadarache, F-13108 Saint Paul-lez-Durance, France,  
romain.le-tellier@cea.fr

January 7, 2021

## Abstract

During a severe accident in a nuclear reactor, the melting of the core may lead to the formation of a multiphase liquid pool (corium) in the vessel lower head. The heat transfer at the boundary with the vessel is affected by diffusive and convective mass fluxes. In particular, the development of Rayleigh-Taylor instabilities influence the thickness of the top metallic layer and therefore the “focusing effect” of the heat flux, which is the main risk for the vessel integrity. We use a Cahn-Hilliard pseudo-binary model to describe the uranium/oxygen/zirconium/iron mixture. The diffusion and the convection are governed by the Cahn-Hilliard equation and the Navier-Stokes equations under the Boussinesq approximation. In this work, the model is isothermal and the buoyancy force is only due to the gradient of chemical composition. The model is solved in three dimensions with a pseudo-spectral code. The initial configuration consists of a light layer of iron-rich fluid above a heavy layer of uranium/oxygen/zirconium mixture. A thin layer of heavier metallic phase lays at the interface and eventually triggers a Rayleigh-Taylor instability. The metallic phase forms a plume which falls downward and then breaks up into droplets due to the Rayleigh-Plateau instability. The phenomenon is alimented by diffusion which generates the heavy metallic phase at the interface. The droplet formation observed in an experiment of corium stratification transient from the literature is qualitatively captured. The mobility, the viscosity and the surface tension are shown to have an influence on the mass transfer.

## KEYWORDS

Severe accident, Corium, Multiphase fluid, Cahn-Hilliard model

## 1 Introduction

The context of this study is that of a severe accident in a light water reactor (LWR). Such an accident can occur if the core is no longer cooled due to a loss of the primary coolant. The core can then melt down and form a hot and radioactive mixture, called corium, whose main components are the molten nuclear fuel ( $\text{UO}_2$ ), the partially oxidized fuel cladding ( $\text{Zr}$ ,  $\text{ZrO}_2$ ) and the vessel steel ( $\text{Fe}$ ,  $\text{Cr}$ ,  $\text{Ni}$ ). Either because of the failure of the core support plate or after the core surrounding structure ablation, corium can flow down to the reactor vessel lower head and accumulate in a “corium pool”. In case of vessel failure, corium can reach the reactor pit. This study is more specifically centered on the “in-vessel-retention” (IVR) strategy, which aims at maintaining the corium within the second confinement barrier, i.e., the vessel. This goal is achieved

by re-flooding the reactor pit (“external reactor vessel cooling”, ERVC) to cool down the vessel wall and avoid melting [1, 2].

The chances of success of the ERVC depend on the thermal flux at the boundary between the corium pool and the vessel. Two types of phenomena impact the behavior of the corium pool and this thermal flux. Firstly, thermochemistry determines the segregation of the multi-component mixture (uranium, oxygen, zirconium, iron, etc.) into various phases [3]. As a matter of fact, the miscibility gap at liquid state in the U-O-Zr-Fe system leads to an oxide phase and a metal one at thermodynamic equilibrium. Secondly, thermal hydraulics determines the heat transfer by diffusion and natural convection operating in the system [4, 5]. The density variations that generate the convection are due to the gradient of the mixture chemical composition and to the gradient of temperature, so that the problem is fully coupled.

One of the key features of this complex phenomenology is the **appearance** of Rayleigh-Taylor instabilities at the interface between the metal and oxide phases, as shown by the MASCA-RCW experiment [6] studying the interaction between a mass of steel and a mass of sub-oxidized corium. Owing to the migration of U and Zr atoms from the sub-oxidized corium (below) to the steel layer (above), a metal phase with a high density was formed at the interface. Eventually, the Rayleigh-Taylor instability led to the destabilization of the interface which resulted in the formation of droplets falling toward the bottom. The **densities** of the metal and oxide phases at thermodynamic equilibrium depend on the overall composition. Below a critical steel quantity, the metal phase is heavier than the oxide one. Above, the metal phase is lighter and an upward movement of the metal phase could be observed. This whole regime, called the stratification transitory regime, must be finely modeled because the main risk for the IVR comes from the “focusing effect”, i.e., the concentration of the heat flux at the lateral surface of the top metallic layer [7].

As discussed in [8] and further illustrated in [9] by code-to-code benchmarks, **large uncertainties still exist in the quantitative assessment of such stratification transients and they have a strong impact on the overall evaluation of vessel wall melt-through under IVR conditions. In order to reduce this uncertainty, the few existing integral models that describe stratification transients in severe accident codes are in need for validation or parameter calibration. “Computational Fluid Dynamics” (CFD) simulations appears as an increasingly valuable tool in order to study pool thermal hydraulics [10, 11] and supplement experimental investigations. In this context, a promising research avenue consists in the modelling of stratification transient phenomena in CFD simulations.**

A Cahn-Hilliard model was proposed to describe the species diffusion in a quaternary (U-O-Zr-Fe) system leading to the phase segregation at thermodynamic equilibrium [12]. This model belongs to the models of phase-field type [13], which are also considered for solidification dynamics [14], spinodal decomposition [15] and multiphase fluids [16], for instance. These diffuse-interface models are useful to address multiphase problems. The state of the system is described by order parameters (following the minimization of a free energy functional), which vary continuously across the interfaces and take constant values in the bulk phases. Solving the associated equations implicitly allows to find the position of the interfaces. Explicit tracking of the moving interfaces is therefore not necessary. In the mentioned corium-related study, the Cahn-Hilliard equation was made consistent with the CALPHAD thermodynamic database [17]. There was nevertheless no coupling with equations of fluid motion or temperature and the convective and thermal phenomena were therefore not captured.

This study is a first step toward the coupling between the thermodynamics model of [12] and thermal hydraulics. The goal is to complete studies performed with integral codes such as [18]. Two main simplifications are used. First, we do not consider a full quaternary model for the U-O-Zr-Fe system but a pseudo-binary model: uranium, oxygen and zirconium are treated as a single component so that the mixture composition is fully described by the molar fraction of iron alone. Second, the temperature is assumed constant. In this work, the (convective) Cahn-Hilliard equation associated to the pseudo-binary model is coupled to the Navier-Stokes equations, and the Boussinesq approximation is used to take into account the variations of the density with the composition. The goal is to show the relevance of such a model to describe the stratification transitory regime. In particular, we wish to show that this model can be representative despite an interface thickness that is much larger than the actual one (the typical feature of phase-field models [19]). A pseudo-spectral code is used for the simulations. **A similar study was previously performed in two dimensions [20], so that it was not able to reproduce the Rayleigh-Plateau instability.**

After this first introductory section, we describe the coupled Cahn-Hilliard and Navier-Stokes system of equations used to model the corium (but that can also be used for any binary Newtonian fluid) and the

considered physical parameters. We then detail the numerical method associated to the pseudo-spectral code. We then present and analyze the simulations of the stratification transitory regime. A parameter study (mobility, viscosity, surface tension) is performed in this section to test the behavior of the model. We finally conclude this work and draw perspectives.

## 2 Problem description and modeling

### 2.1 Problem description

We consider a system that is inspired by the MASCA-RCW experiment [6]. In this experiment, **about** 45.3 kg of sub-oxidized corium was put in presence of **about** 4.3 kg of steel in a crucible at high temperature. The experiment was stopped after 20', a time sufficient for the diffusion of the components to notably progress but not sufficient to reach a steady regime: the system was in the stratification transitory regime at the end of the experiment. The analysis of the post-mortem ingot (**Fig. 1**) revealed that the metal phase was split into: a light metal phase above the oxide phase (**legend 7**); inclusions of heavy metal phase in the oxide phase (**legend 4**); a heavy metal phase under the oxide phase (**legend 2**). The physical explanation for this observation is that U and Zr atoms migrate from the sub-oxidized corium to the steel, forming a heavy metal phase at the interface. The heavy metal phase above the oxide phase then generates Rayleigh-Taylor instabilities, which lead to the formation droplets of heavy metal phase relocalizing at the bottom.

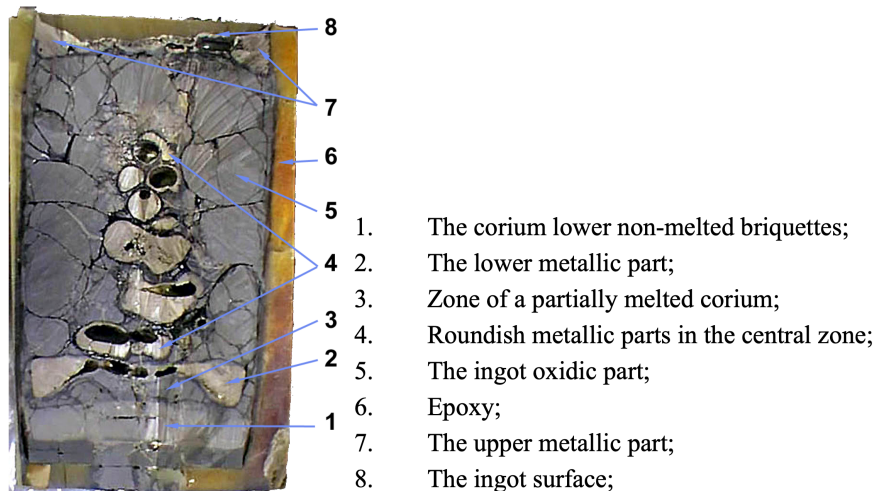


Figure 1: Cross-section of the MASCA-RCW post-mortem ingot [6].

In our case, the initial state consists of a phase of pure iron above a phase of primarily oxygen, uranium and zirconium. Thermochemistry leads to the segregation of this U-O-Zr-Fe system into an oxide phase and a metal one at thermodynamic equilibrium. The molar fractions, the volume and the mass density of each phase of the considered system at the initial state and at thermodynamic equilibrium at 3000 K are given in Table 1. Note that at the initial state, the metal phase (pure iron) is lighter than the oxide phase so that the system is mechanically stable. Nevertheless, diffusion modifies the composition profile, starting from the area close to the interface. At the equilibrium state, the metal phase is heavier than the oxide phase. Thus, once diffusion has sufficiently progressed at the interface, Rayleigh-Taylor instabilities can develop. The transitory of stratification revealed by the MASCA-RCW experiment can therefore be captured in this system.

### 2.2 Modeling

The problem is solved in three dimensions, with the gravity force  $\mathbf{g} = -g\mathbf{e}_z$ ,  $g > 0$ . The computational domain is the rectangular box

$$\Omega = \left\{ (x, y, z) \in \left[ -\frac{L}{2}, \frac{L}{2} \right] \times \left[ -\frac{L}{2}, \frac{L}{2} \right] \times \left[ -\frac{7L}{2}, \frac{L}{2} \right] \right\}. \quad (1)$$

	Initial state		Equilibrium state (3000 K)	
	Oxide phase	Metal phase	Oxide phase	Metal phase
$x_{Fe}$	$8.11 \cdot 10^{-6}$	1	$1.88 \cdot 10^{-3}$	$6.16 \cdot 10^{-1}$
$x_O$	$5.80 \cdot 10^{-1}$	0	$6.28 \cdot 10^{-1}$	$2.23 \cdot 10^{-2}$
$x_U$	$2.29 \cdot 10^{-1}$	0	$1.99 \cdot 10^{-1}$	$2.06 \cdot 10^{-1}$
$x_{Zr}$	$1.91 \cdot 10^{-1}$	0	$1.70 \cdot 10^{-1}$	$1.55 \cdot 10^{-1}$
$V$ (m <sup>3</sup> )	$5.75 \cdot 10^{-3}$	$6.55 \cdot 10^{-4}$	$4.91 \cdot 10^{-3}$	$1.43 \cdot 10^{-3}$
$\rho$ (kg · m <sup>-3</sup> )	$8.25 \cdot 10^3$	$6.97 \cdot 10^3$	$7.98 \cdot 10^3$	$9.01 \cdot 10^3$

Table 1: Composition, volume and mass density of the corium phases at thermodynamic equilibrium at 3000 K (based on calculations performed with the NUCLEA'09 database [21] and species density laws implemented in the PROCOR code [22]).

The side of an horizontal slice is the diameter of the MASCA-RCW setup:  $L = 0.176$  m. We use  $g = 9.81 \text{ m} \cdot \text{s}^{-2}$ , the standard acceleration of gravity.

### 2.2.1 Pseudo-binary model approximation

Although the system is composed of four elements, it segregates into only two phases: an oxygen-rich phase and an iron-rich phase. The pseudo-binary approximation consists in considering that the oxygen, the uranium and the zirconium in the oxide phase keep their relative proportion while they transfer to the metal phase. This approximation is inaccurate, especially for oxygen, but allows a first range of qualitative simulations. Under this assumption, corium can be modeled as a fluid mixture of two components 1 (uranium, oxygen, zirconium) and 2 (iron). The chemical composition of the pseudo-binary model is given by the molar fraction of iron  $x_{Fe}$ , denoted by  $c$  in the following. In this work, we assume a constant molar volume.

### 2.2.2 Free energy functional

Following the theory of Cahn and Hilliard [23], the diffusion is governed by the minimization of a free energy functional

$$F[c] = \int \left( f_0(c) + \frac{\epsilon}{2} (\nabla c)^2 \right) dV, \quad (2)$$

where  $f_0$  is the free energy by unit volume of an homogeneous system and  $\epsilon$  a positive constant.  $f_0$  is of the form

$$f_0(c) = A(c - c_{ox})^2(c - c_{met})^2, \quad (3)$$

where  $A$  is a positive constant and  $c_{ox} = 1.88 \cdot 10^{-3}$  and  $c_{met} = 6.16 \cdot 10^{-1}$  are the molar fraction of iron in the oxide phase and the metal phase at thermodynamic equilibrium (3000 K), respectively. The double-well shape of  $f_0/A$  is illustrated in Fig. 2.

This free energy expression leads to a theoretical solution for the equilibrium composition profile with  $c = c_{ox}$  and  $c = c_{met}$  in the bulk phases and a hyperbolic tangent profile at the interface. The interface thickness  $w_{int}$  and the surface tension  $\gamma$  at equilibrium associated to Eqs. (2) and (3) are given by

$$w_{int} = \frac{1}{c_{met} - c_{ox}} \sqrt{\frac{8\epsilon}{A}}, \quad \gamma = \sqrt{\frac{A\epsilon}{18}} (c_{met} - c_{ox})^3. \quad (4)$$

Note that these equalities can be reversed to express  $A$  and  $\epsilon$  as functions of  $w_{int}$  and  $\gamma$ :

$$A = \frac{12\gamma}{(c_{met} - c_{ox})^4 w_{int}}, \quad \epsilon = \frac{3w_{int}\gamma}{2(c_{met} - c_{ox})^2}. \quad (5)$$

It is numerically impossible to use an interface thickness as small as in nature (of the order of Angstroms) because it would require an extremely fine mesh. Here, it is taken small compared to the length scale of the

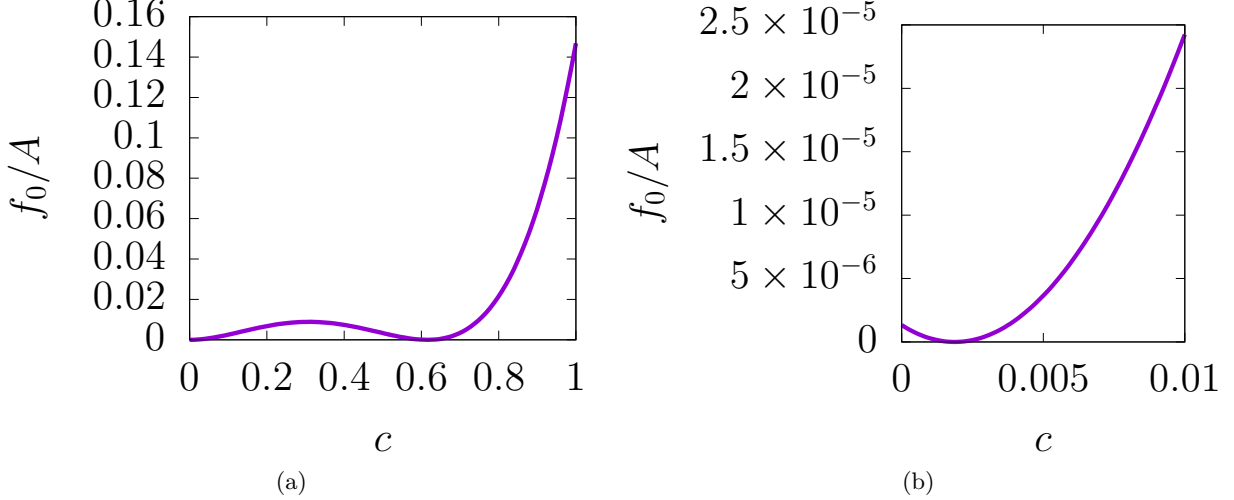


Figure 2: (a) Corium homogeneous free energy as a function of the molar fraction of iron. (b) Zoom close to zero.

problem:  $w_{int} = L/20$ . The order of magnitude of the surface tension is estimated by using the formula of Girifalco and Good [24], valid under an assumption of constant molar volume:

$$\gamma_0 = \gamma_{UO_2} + \gamma_{Fe} - 2\sqrt{\gamma_{UO_2}\gamma_{Fe}} \approx \mathbf{0.385} \text{ N} \cdot \text{m}^{-1}, \quad (6)$$

where  $\gamma_{UO_2} = \mathbf{0.536} \text{ N} \cdot \text{m}^{-1}$  and  $\gamma_{Fe} = \mathbf{1.83} \text{ N} \cdot \text{m}^{-1}$  are the surface tensions of liquid uranium oxide and of liquid iron, based on [25, pp. 31 and 150]<sup>1</sup>. In the simulations, the surface tension is varied in the range  $0.7\gamma_0 \leq \gamma \leq 1.2\gamma_0$ .

### 2.2.3 Composition and velocity equations

We consider the diffusion equation of Cahn-Hilliard [26], with an additional convective term, coupled with the equations of Navier-Stokes under the Boussinesq approximation:

$$\partial_t c + \mathbf{v} \cdot \nabla c = M \Delta \mu, \quad (7)$$

$$\partial_t \mathbf{v} + \nabla \cdot (\mathbf{v} \otimes \mathbf{v}) = -\frac{1}{\rho_1} \nabla p + \frac{\eta}{\rho_1} \Delta \mathbf{v} - \frac{1}{\rho_1} \left( c - \frac{c_{ox} + c_{met}}{2} \right) \nabla \mu + \frac{\rho(c) - \rho_1}{\rho_1} \mathbf{g}, \quad (8)$$

$$\nabla \cdot \mathbf{v} = 0, \quad (9)$$

where  $\mathbf{v}$  is the velocity,  $M$  the mobility,  $\mu = \delta F / \delta c$  the diffusion potential<sup>2</sup> (the associated term in Eq. (8) represents the capillary force),  $\rho_1$  the density of component 1,  $p$  the pressure,  $\eta$  the dynamic viscosity (assumed uniform) and  $\mathbf{g}$  the gravity. The gradient part of the gravity force is absorbed in the pressure gradient, which induces the change of variable (already present in Eq. (8))

$$p \leftarrow p - \rho_1 \mathbf{g} \cdot \mathbf{x}, \quad (10)$$

where  $\mathbf{x} = (x, y, z)$  is the position vector.

The mobility value must be chosen accordingly with the interface thickness value, which is much larger than in nature, to preserve the characteristic diffusion time. To establish the order of magnitude of  $M$ , we use a formula analogous to [19, Eq. (44)]:

$$M_0 = \frac{w_{int}}{w_{int,ref}} M_{ref}, \quad (11)$$

<sup>1</sup>The value of  $\gamma_{UO_2}$  is for a temperature of 3000 K while the value of  $\gamma_{Fe}$  is for the melting point.

<sup>2</sup>The diffusion potential is defined as the difference between the chemical potentials of components 2 and 1:  $\mu = \mu_2 - \mu_1$ .

where  $w_{int,ref} = 10^{-9}$  m and  $M_{ref} = 10^{-18} \text{ J}^{-1} \cdot \text{m}^5 \cdot \text{s}^{-1}$  are the orders of magnitude of the interface thickness and the mobilities in the corium. The value of  $M_{ref}$  is established by considering an approximation of the formula [12, Eq. (2.87)]:

$$M_{ref} = \frac{V_m}{RT} (D_U + D_{Zr} + D_O + D_{Fe}), \quad (12)$$

where  $V_m = 10^{-5} \text{ m}^3 \cdot \text{mol}^{-1}$  is the molar volume (typical value from CALPHAD data),  $R = 8.31 \text{ J} \cdot \text{mol}^{-1} \cdot \text{K}^{-1}$  the molar ideal gas constant,  $T = 3000$  K and  $D_U/D_{Zr}/D_O/D_{Fe}$  are the self-diffusion coefficients. The latter are obtained through Arrhenius laws [12, Eq. (3.37), Tables 3.2-3.3, pp. 81-82] for U and O in liquid  $\text{UO}_2$ ,

$$\begin{aligned} D_U &= 3.9 \times 10^{-4} \exp(-5eV/(k_B T)) \approx 1.55 \times 10^{-12} \text{ m}^2 \cdot \text{s}^{-1}, \\ D_O &= 6.6 \times 10^{-8} \exp(-0.8eV/(k_B T)) \approx 2.99 \times 10^{-9} \text{ m}^2 \cdot \text{s}^{-1}, \end{aligned} \quad (13)$$

where  $eV = 1.60 \times 10^{-19}$  J is an electronvolt and  $k_B = 1.38 \times 10^{-23} \text{ J} \cdot \text{K}^{-1}$  the Boltzmann constant, and assuming that  $D_{Zr} = D_{Fe} = D_U$  (in the absence of data regarding Zr and Fe in corium). The formula in Eq. (11) leads to a value of order  $10^{-11} \text{ J}^{-1} \cdot \text{m}^5 \cdot \text{s}^{-1}$  for  $M_0$ . In the simulations, the mobility is varied in the range  $0.8M_0 \leq M \leq 2.5M_0$ .

The construction of the density law  $\rho(c)$  is based on the densities of the mixture at the initial and thermodynamic equilibrium state. A polynomial function is used to interpolate between these points:

$$\rho(c) = \begin{cases} 7979.94 & \text{if } c \leq c_{ox}, \\ 7979.97 - 27.75c + 7416.06c^2 - 6154.38c^3 - 2247.48c^4 & \text{if } c > c_{ox}, \end{cases} \quad (14)$$

see Fig. 3. The polynomial is chosen such that  $\frac{d\rho}{dc}(c_{ox}) = \frac{d\rho}{dc}(c_{met}) = 0$ . And as it can be seen in Fig. 3, we have chosen to disregard the first point ( $c = 8.11 \cdot 10^{-6}$ ) when building the interpolation polynomial because the non monotonicity of the density close to 0 leads to spurious flow effects that are not physical and that are related to the simplifications introduced by the use of a pseudo-binary model (see Table 1). To this purpose as well, the polynomial is extended by a constant value for  $c \leq c_{ox}$ . Physically, the difference in the densities of the oxide phase at initial state and at equilibrium is associated to the change in U, Zr and O content (in particular, the oxidation degree increases at equilibrium and leads to a lower mass density). We use  $\rho_1 = 8.25 \cdot 10^3 \text{ kg} \cdot \text{m}^{-3}$ , the density of the initial oxide phase, as the reference density of the Boussinesq approximation. With the physical properties considered in this work, the last two terms on the right-hand-side of Eq. (8) have similar magnitude.

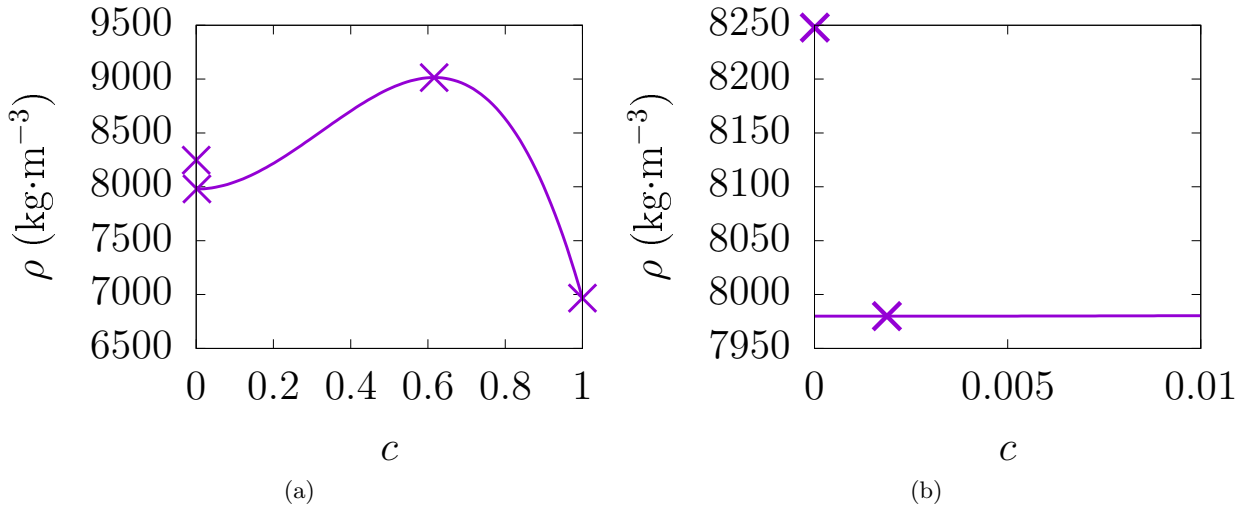


Figure 3: (a) Corium density as a function of the molar fraction of iron. (b) Zoom close to zero. The cross symbols represent the initial and equilibrium values in each phase.

The dynamic viscosity of the corium at the considered temperature is of order  $10^{-3} - 10^{-2} \text{ Pa} \cdot \text{s}$ . Using such a viscosity value leads to a strong velocity in the nonlinear regime of the Rayleigh-Taylor instability,

which causes a numerical convergence issue for the considered parameters. We set a stronger viscosity value  $\eta$  between 8 and 18 Pa·s to overcome this convergence issue. **The value of the viscosity is nevertheless sufficiently low for the convection step of the process (fall of heavy metal phase by Rayleigh-Taylor instability) to be short compared to the diffusion step (formation of the heavy metal phase at the interface by interdiffusion). As a result, as confirmed by the numerical simulations, the volume of iron that falls at the bottom is likely to be limited by mobility and not by viscosity as long as the time scale separation between flow and interdiffusion is sufficient.**

## 2.2.4 Initial condition

Owing to the assumption of periodic boundary conditions necessary for the use of the spectral method, we need to consider that  $\Omega$  is part of an infinite and periodic domain, see Fig. 4a. The initial composition is

$$c_0(x, y, z) = \begin{cases} \frac{1}{2} \left( 1 - \tanh \left( \frac{2(z + 7L/2)}{w_{int}} \right) \right) & \text{if } -\frac{7L}{2} \leq z < -\frac{7L}{4}, \\ \frac{1}{2} \left( 1 + \tanh \left( \frac{2(z + \zeta_0 \exp(-0.5(x^2 + y^2)/\sigma_0^2))}{w_{int}} \right) \right) & \text{if } -\frac{7L}{4} \leq z < \frac{L}{4}, \\ \frac{1}{2} \left( 1 - \tanh \left( \frac{2(z - L/2)}{w_{int}} \right) \right) & \text{if } \frac{L}{4} \leq z \leq \frac{L}{2}, \end{cases} \quad (15)$$

where  $\zeta_0 = \sigma_0 = 0.5 \times 10^{-4}L$ . This expression defines a smooth profile between the bulk phases at  $z = 0$ , but also at  $z = -7L/2$  (bottom boundary) and  $z = L/2$  (top boundary), see Fig. 4b. The initial composition profile is such that a thin layer of matter with a composition close the equilibrium composition of the metal phase ( $c \approx c_{met}$ ) lays at the top of the initial oxide phase (see at  $z = 0$ ). The density law is such that this thin layer of matter has a stronger density than the matter underneath, see Fig. 4c. The thickness of this layer is sufficient for the configuration to be mechanically unstable. The parameter  $\zeta_0$  enforces a tiny perturbation necessary for the Rayleigh-Taylor instabilities to develop. The initial perturbation of the interface is a gaussian centered in the center of the mid-plane. Note that the initial composition profile does not respect the proportion of oxide and metal phase of the MASCA-RCW experiment (Table 1), but since we are only interested in the transitory regime, this is not relevant. The system is initially at rest, so the initial velocity is zero.

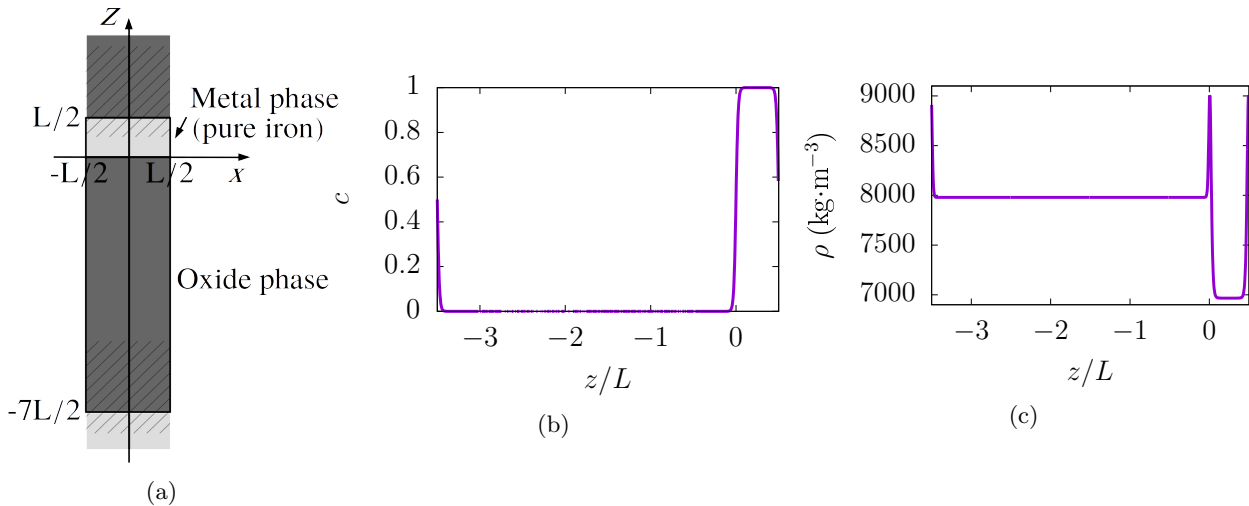


Figure 4: (a) Initial composition field (the unstable interface is at  $z = 0$ ); the dashed area represent the area of zero-gravity which stabilize the top and bottom interfaces. (b) Initial composition profile. (c) Initial density profile.

Due to the periodicity of the infinite domain, the bottom fluid is lighter than the top fluid at the bottom and top boundaries, which are therefore unstable. To avoid Rayleigh-Taylor instabilities at these boundaries,

we numerically cancel the gravity in the regions  $z < -5L/2$  and  $z > L/4$ . The domain is higher than the actual system so that the periodic boundary conditions, naturally enforced by the spectral method, have limited effect on the development of the instabilities close to the interface of interest.

### 3 Numerical method

The solution fields are assumed periodic of periods  $N_x\Delta x = L$  in the  $x$  direction,  $N_y\Delta x = L$  in the  $y$  direction and  $N_z\Delta x = 4L$  in the  $z$  direction, where  $\Delta x > 0$  is the mesh size and  $N_x \in \mathbb{N}$  (resp.  $N_y/N_z \in \mathbb{N}$ ) is the number of Fourier modes used in the  $x$  (resp.  $y/z$ ) direction. The solving consists in computing the  $N_x \times N_y \times N_z$  Fourier coefficients associated to the solution fields at every time iteration. An implicit Euler time scheme is used. The code is said pseudo-spectral because the non-linear terms are treated explicitly. The model and the code were used in the study of the Rayleigh-Taylor instability [27] and the agreement between the numerical results and well established theoretical predictions was shown to be excellent. To obtain a smooth solution, we use at least 10 cells inside the diffuse interface thickness. We use  $\Delta x = w_{int}/12$  ( $N_x = N_y = 240$ ,  $N_z = 960$ ) in every case except for  $M \geq 2M_0$  where we use  $\Delta x = w_{int}/10$  ( $N_x = N_y = 200$ ,  $N_z = 800$ ) because a stronger mobility increases numerical stability. The time step used to reach convergence varies in each case and during the simulations but is of the form  $\tau = 0.05/2^k$  and such that

$$\frac{v_{max}\tau}{\Delta x} \leq C, \tag{16}$$

where  $v_{max}$  is the maximum value of the velocity (in norm) in the system and  $C = 0.025$  or  $0.05$  in the step-by-step regime and  $C = 0.1, 0.125$  or  $0.25$  in the continuous regime. Practically, the time step is bounded by  $1.95313 \times 10^{-4} \text{ s} \leq \tau \leq 0.05 \text{ s}$ .

## 4 Results

The simulations are performed over a physical time of 600 s ( $10^3$ ), which is sufficient for several droplets to form at the interface and fall. We first describe the formation of droplets, in the case  $M = M_0$ ,  $\eta = 10 \text{ Pa} \cdot \text{s}$  and  $\gamma = \gamma_0$ , and then discuss the effect of parameters  $M$ ,  $\eta$  and  $\gamma$ .

### 4.1 Droplet formation

At the beginning of the transient, the interface is flat from a macroscopic point of view. The tiny enforced perturbation and the Rayleigh-Taylor instability eventually lead to the formation of a mass of heavy metal phase at the interface ( $t \approx 150 \text{ s}$ ) that falls vertically, forming a plume, into the oxide phase. Due to the Rayleigh-Plateau instability [28], the plume breaks into droplets, which stop when they reach the region of zero gravity. The first fall of metal phase leads others that follow a similar path. As a matter of fact, diffusion leads to the formation of metal phase at thermodynamic equilibrium at the interface. As said, this phase is more dense than the oxide phase underneath and is consequently regularly evacuated by convection toward the bottom. The droplets then gather in the region of zero gravity. Fig. 5 shows the formation of the plume and the pinch-off of droplets. Note that surface tension destabilizes the plume, after several droplets have detached, and reinstate a flat interface. The shape of the plume and the formation of droplets (a primary one followed by satellite ones) are similar to the computational results obtained in [29] for instance. The droplet formation observed in Fig. 1 is qualitatively reproduced in this simulation, even in terms of droplet size. The diameter of the leading drop is about one tenth of the setup diameter, similar to the droplets in Fig. 1. The satellite droplets (and the droplets obtained in the continuous regime, see next) have a smaller diameter than the experiment droplets though.

In order to characterize the mass transfer in the system, we study the time evolution of the flow of iron toward the bottom at two locations:

$$Q_{V,top}(t) = - \int_{x=-L/2}^{L/2} \int_{y=-L/2}^{L/2} c \left( x, y, -\frac{L}{4}, t \right) v_z \left( x, y, -\frac{L}{4}, t \right) dx dy \tag{17}$$

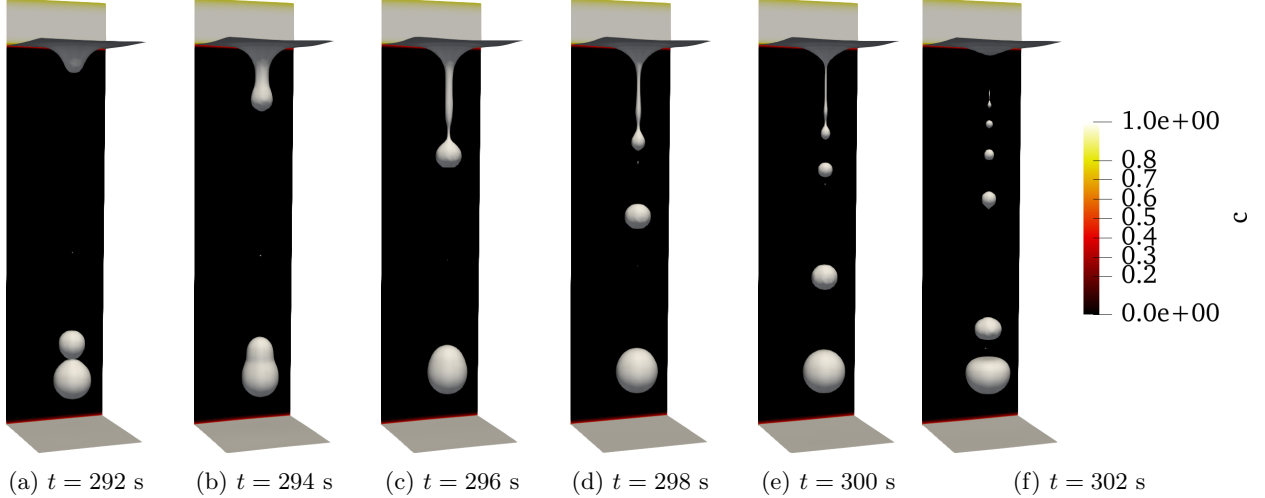


Figure 5: Composition field and iso-surface  $c = 0.5$  during the fall and pinch-off of metal phase droplets for  $M = M_0$ ,  $\eta = 10 \text{ Pa} \cdot \text{s}$  and  $\gamma = \gamma_0$ .

is calculated at the plane of height  $z = -L/4$ , i.e., just under the unstable interface, and

$$Q_{V,bot}(t) = - \int_{x=-L/2}^{L/2} \int_{y=-L/2}^{L/2} c \left( x, y, -\frac{9L}{4}, t \right) v_z \left( x, y, -\frac{9L}{4}, t \right) dx dy \quad (18)$$

is calculated at the plane of height  $z = -9L/4$ , i.e., just above the zero-gravity region. We also consider the accumulated volume of iron under these planes  $V_{top}$  and  $V_{bot}$ , i.e., the time integration of  $Q_{V,top}$  and  $Q_{V,bot}$ . Since  $Q_{V,bot}$  is computed close to the zero-gravity region,  $V_{bot}$  can be seen as the accumulated volume of iron at the bottom. We present the time evolution of these quantities in Fig. 6. The fall of metal phase corresponds to peaks in the curves of  $Q_{V,top}$  and  $Q_{V,bot}$ . One can notice that, as mentioned, the falls of metal phase arise at regular time intervals. One can also notice that the flow is different close to the unstable interface ( $Q_{V,top}$ ) and close to the zero-gravity region ( $Q_{V,bot}$ ). This is due to the fact that the metal phase forms a plume at the beginning of the fall, which breaks into droplets at mid-height approximately. One peak in the curve of  $Q_{V,top}$  (resp.  $Q_{V,bot}$ ) corresponds to a step in that of  $V_{top}$  (resp.  $V_{bot}$ ). The steps in the curve of  $V_{top}$  are smoother than that of  $V_{bot}$ , due to the mentioned change plume/droplets during the fall, but they logically lead to the same amount at the end. In the following, we focus on  $V_{bot}$  because the presence of small crenelations shows the formation of droplets along the plume. **Note in Fig. 6 that the periods of fall of heavy metal phase are short compared to the periods of growth of the heavy metal layer at the interface, even though the corium viscosity (which impacts the flow speed) is over-estimated in the model. Thus, the flow of heavy metal phase is mainly controlled by diffusion.**

We find it important to note that the accumulated volume of iron is approximately  $350 \text{ cm}^3$  at  $t = 600 \text{ s}$  ( $10'$ ). Indeed, it corresponds to about  $2.4 \text{ kg}$  of iron. One would expect the fallen mass of iron to reach about  $5.3 \text{ kg}$  in  $22'$ , the length of the MASCA-RCW experiment. This value is consistent with the mass of heavy metal phase of about  $4.3 \text{ kg}$  relocalized at the bottom in the experiment at the end of it. The simulation over-predicts the speed of the formation of the heavy metal phase layer. However, as shown next, the process strongly depends on the mobility and calibrating the mobility value should help to improve the prediction. A one-at-a-time sensitivity analysis is now reported for the mobility, viscosity and surface tension parameters.

## 4.2 Influence of the mobility

We first study the influence of the mobility. We fix the viscosity at  $\eta = 10 \text{ Pa} \cdot \text{s}$  and the surface tension at  $\gamma = \gamma_0$  and use various values of  $M$ . The time evolution of  $V_{bot}$  for every  $M$  is shown in Fig. 7. As one can see, when  $M$  is increased, the step-by-step shape of the curve is changed into a linear shape. This is due to the fact that the metal phase flows down in a continuous way instead of by steps. The flow corresponding to  $M = 1.5M_0$  is shown in Fig. 8a, which can be compared to Fig. 5f. In this case, the initial perturbation leads

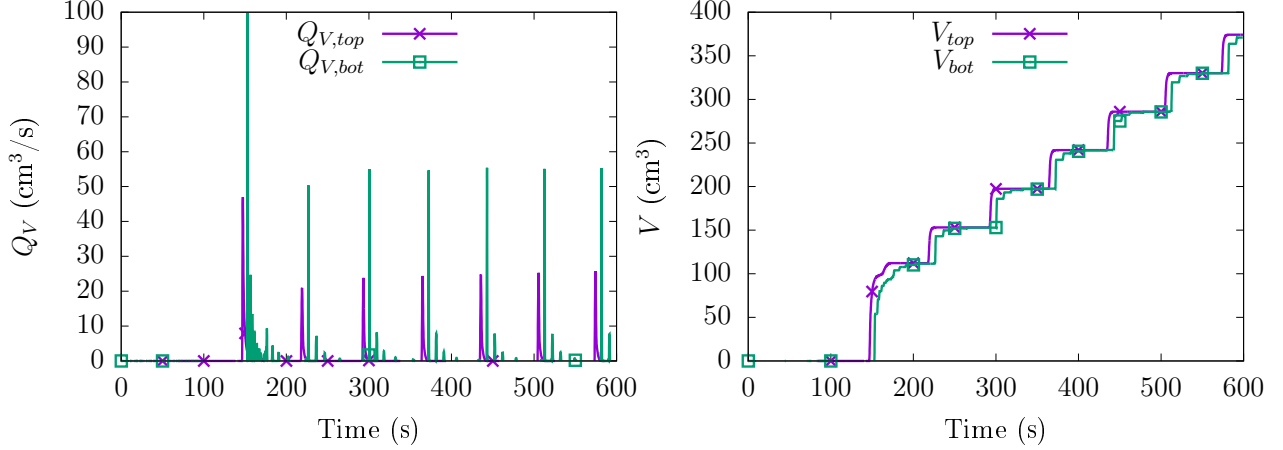


Figure 6: Flow of iron toward the bottom and accumulated volume of iron as a function of time for  $M = M_0$ ,  $\eta = 8 \text{ Pa} \cdot \text{s}$  and  $\gamma = \gamma_0$ .

to a plume of metal phase that is located at the corners of the domain. The flow of metal phase does not stop. Droplets are still formed at the end of the plume by Rayleigh-Plateau instability though. One can suggest a physical explanation for this observation. Increasing the mobility value speeds up diffusion. Therefore, more heavy metal phase can be generated in a given time at the interface, and the plume has more inertia. For high values of  $M$ , the inertia is sufficiently strong to overcome surface tension and to stabilize the plume during a longer period of time. Note that in the case  $M = 1.4M_0$ , the flow regime transitions from a continuous regime to a step-by-step regime around  $t = 450 \text{ s}$ . The regime transition probably explains the irregular steps, which might become regular at later times, in this case. Note also in Fig. 7 that, when  $M$  is increased, convection starts earlier and the time interval between the falls of metal phase in the step-by-step regime is reduced. Diffusion strengthening, by accelerating the generation of heavy metal phase at the interface, increases the growth rate of the Rayleigh-Taylor instability.

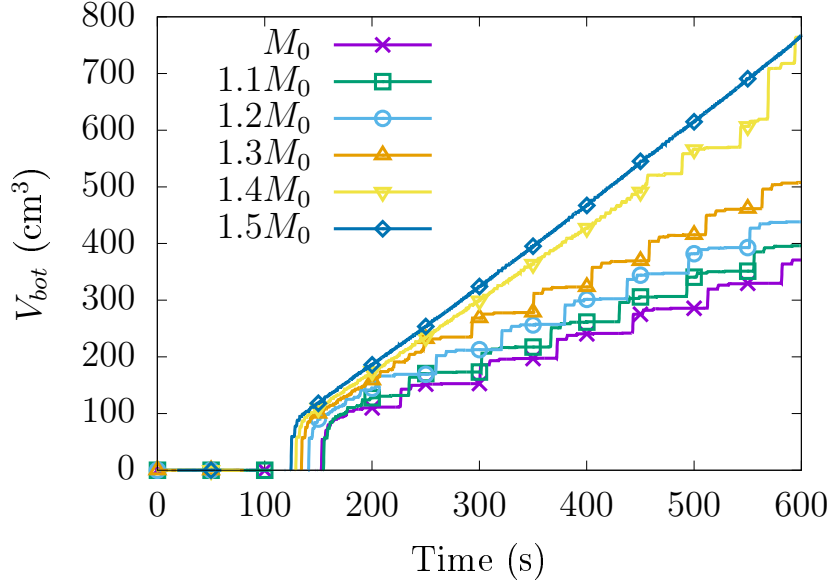


Figure 7: Accumulated volume of iron at the bottom as a function of time for  $\eta = 10 \text{ Pa} \cdot \text{s}$ ,  $\gamma = \gamma_0$  and various values of  $M$ .

We could expect the accumulated volume of iron at the bottom to depend linearly on the mobility. As a matter of fact, the diffusion flux of matter is proportional to  $M$  in the Cahn-Hilliard equation, see Eq. (7).

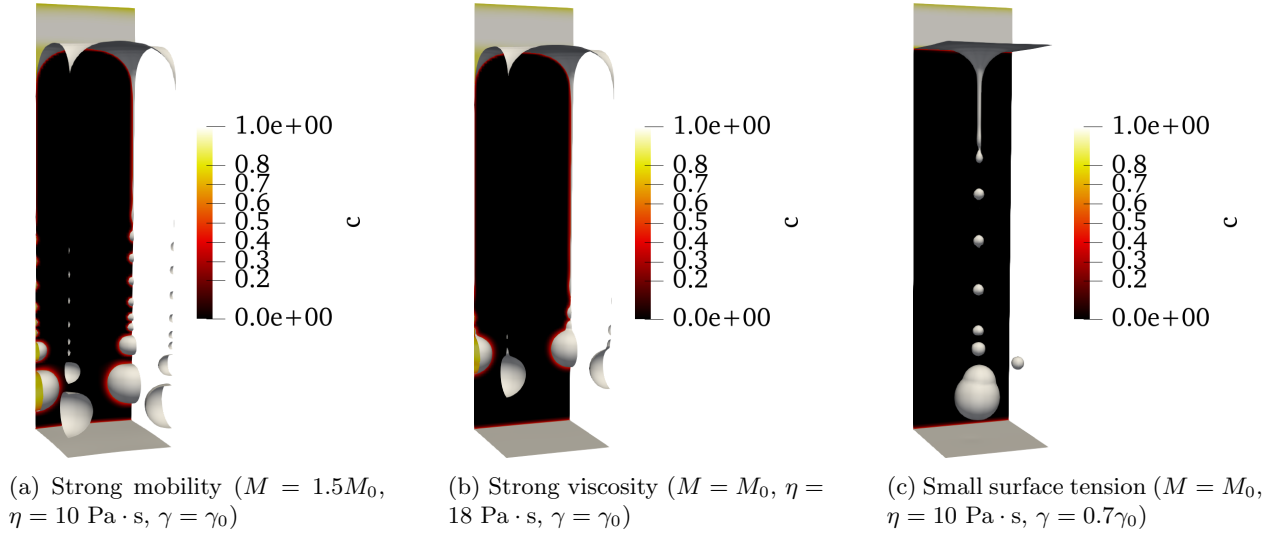


Figure 8: Composition field and iso-surface  $c = 0.5$  during the fall and pinch-off of metal phase droplets in the continuous regime ( $t = 302 \text{ s}$ ).

One can nevertheless observe in Fig. 7 that this is not exactly the case. There is a much larger gap between the curves  $M = 1.3M_0$  and  $M = 1.4M_0$  than between the other curves (at  $t = 400 \text{ s}$  for instance). We represent the accumulated volume of iron at the bottom at  $t = 600 \text{ s}$  as a function of the ratio  $M/M_0$  in Fig. 9. The curve is linear except in the transition between regimes ( $M/M_0 \approx 1.4$ ). The regime change produces a nonlinear effect on the relocalization of the iron. The continuous regime **leads to a faster mass transport** than the step-by-step regime.

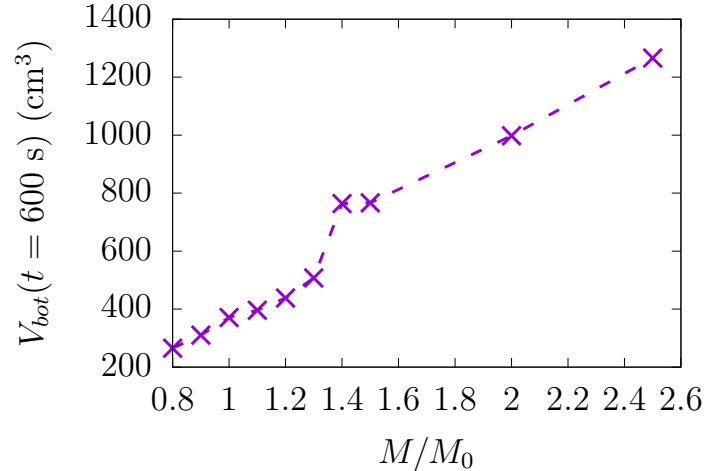


Figure 9: Accumulated volume of iron at the bottom at  $t = 600 \text{ s}$  as a function of  $M/M_0$  ( $\eta = 10 \text{ Pa} \cdot \text{s}$ ,  $\gamma = \gamma_0$ ).

### 4.3 Influence of the viscosity

We now study the influence of the viscosity. We fix the mobility at  $M = M_0$  and the surface tension at  $\gamma = \gamma_0$  and use various values of  $\eta$ . The time evolution of  $V_{bot}$  for every  $\eta$  is shown in Fig. 10. As one can see, when  $\eta$  is increased, there is a regime transition from a step-by-step regime to a continuous regime (the flow corresponding to  $\eta = 18 \text{ Pa} \cdot \text{s}$  is shown in Fig. 8b). The viscous force is therefore able to stabilize the plume during a longer period of time. Note also that the onset of convection is delayed when  $\eta$  is increased.

It is consistent because when the viscosity is increased, the growth rate of the Rayleigh-Taylor instability is reduced (this can be deduced from the theoretical predictions of [30] for instance).

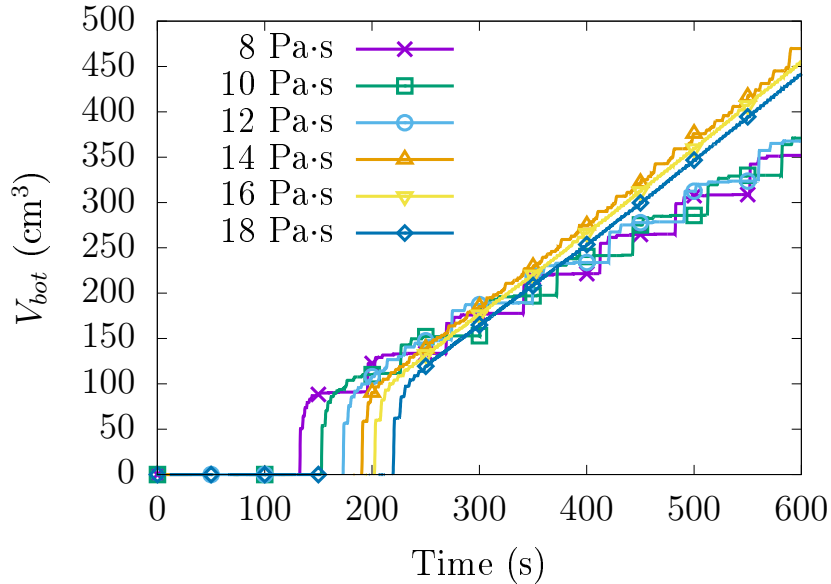


Figure 10: Accumulated volume of iron at the bottom as a function of time for  $M = M_0$ ,  $\gamma = \gamma_0$  and various values of  $\eta$ .

One can also observe in Fig. 10 that when  $\eta$  is increased, the accumulated volume of iron at the bottom might be slightly increased (see at  $t = 600$  s for instance). This is not intuitive because one could imagine that viscosity should slow down the mass transfer and therefore also the relocalization of the iron. This happens to be questionable when looking at the curves of  $\eta = 14, 16$  and  $18 \text{ Pa} \cdot \text{s}$ . The slope of the curve, once the plume is established, seems unchanged when  $\eta$  is increased, meaning that  $Q_{V,bot}$ , the flow of iron, is unchanged. We can assume that the increase of  $V_{bot}$  at a given time with  $\eta$  is an effect of the regime transition. As already mentioned, the continuous regime is more efficient than the step-by-step regime. Apparently, the relocalization of the iron is eventually faster in case of a slow but steady flow of matter (continuous regime, strong  $\eta$ ) than in the case of a fast but intermittent one (step-by-step regime, low  $\eta$ ). **Let us note that viscosity seems to have little influence on the volume of fallen iron during a convection step in case of discontinuous regime (low values of  $\eta$ ). The heights of the steps for  $\eta = 8, 10$  and  $12 \text{ Pa} \cdot \text{s}$  are indeed approximately identical in the steady-state regime (late time).**

#### 4.4 Influence of the surface tension

We finally study the influence of the surface tension. We fix the mobility at  $M = M_0$  and the viscosity at  $\eta = 10 \text{ Pa} \cdot \text{s}$  and use various values of  $\gamma$ . The time evolution of  $V_{bot}$  for every  $\gamma$  is shown in Fig. 11. As one can see, when  $\gamma$  is increased, there is a regime transition from a continuous regime to a step-by-step regime (the flow corresponding to  $\gamma = 0.7 \gamma_0$  is shown in Fig. 8c). The strengthening of the capillary force avoids the appearance of a continuous plume. Note also that the onset of convection is delayed and the time interval between the falls of metal phase in the step-by-step regime is increased when  $\gamma$  is increased. This is consistent because when the surface tension is increased, the growth rate of the Rayleigh-Taylor instability is reduced (this can again be deduced from the theoretical predictions of [30]). Note also that when the continuous regime is changed into a step-by-step regime ( $\gamma \geq 0.8\gamma_0$  approximately), the time-average flow of iron is reduced. This observation confirms that a continuous regime is more efficient regarding the relocalization of the iron than a step-by-step regime.

**While the mobility is the key parameter that governs the mass transport, the transition between the discontinuous flow regime and the continuous flow regime has effects that cannot be neglected. It is therefore important to be able to predict when this transition is likely to happen. To this purpose, the use of the**

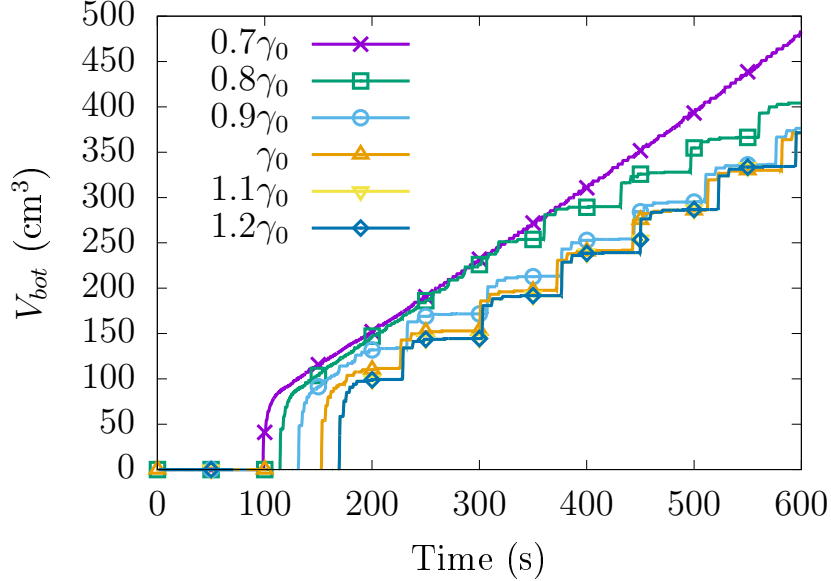


Figure 11: Accumulated volume of iron at the bottom as a function of time for  $M = M_0$ ,  $\eta = 10 \text{ Pa} \cdot \text{s}$  and various values of  $\gamma$ .

capillary number  $N_{ca} = \eta V_{ref} / \gamma$ , where  $V_{ref}$  is a characteristic velocity scale ( $V_{ref} = 10^{-2} \text{ m} \cdot \text{s}^{-1}$  for instance, considering the orders of magnitude of the flow of iron and of the size of the system), which compares the viscous and surface tension forces, should be relevant. The regime change appears around  $N_{ca} \approx 0.3 - 0.4$  in both Figs. 10 & 11. One can expect that below this threshold value of  $N_{ca}$ , the flow regime will be discontinuous, and that it will be continuous above. The Ohnesorge number  $O_h = \eta^2 / (\rho_1 \gamma L_{ref})$ , where  $L_{ref}$  is a characteristic lengthscale ( $L_{ref} = L$  for instance) [31], is also of interest because it takes into account viscous, surface tension and inertial effects. This has to be confirmed by simulations over larger parameter ranges.

## 5 Conclusion

We have presented a simple three-dimensional and isothermal model for the transitory stratification regime that occurs in the corium pool in the context of the IVR strategy. The model splits the main chemical elements in presence into two components (U, O, Zr on one side and Fe on the other), i.e., treats the corium as a binary fluid, and couples the convective Cahn-Hilliard equation and the Navier-Stokes equations under the Boussinesq approximation. The problem is simulated with a pseudo-spectral code in a domain with periodic boundary conditions.

The Rayleigh-Taylor instability at the interface between the iron and the oxidized corium leads to the formation of a plume of heavy metal phase that flows toward the bottom. The plume breaks into droplets due to the Rayleigh-Plateau instability. We were therefore able to reproduce a droplet regime similar to the one shown by the MASCA-RCW experiment. The plume of heavy metal phase is affected by the balance between three forces: inertial forces (depending on the mobility), viscous forces (depending on the viscosity) and capillary forces (depending on the surface tension). The inertial forces depend on the mobility because it controls diffusion and therefore the rate of formation of heavy metal phase at the interface. While inertial forces and viscous forces tend to stabilize the plume, capillary forces tend to destabilize it. Therefore, changing the parameters of  $M$ ,  $\eta$  and  $\gamma$  lead to a regime where the plume of heavy metal phase is either continuous or discontinuous. The effects of these parameters on the regime are similar or reciprocal. The flow could be characterized by a dimensionless number, such as the capillary number or the Ohnesorge number.

The viscosity of corium is over-estimated by several orders of magnitude because of numerical difficulties. Nevertheless, for low enough values of the viscosity, the fall of heavy metal phase is sufficiently fast for diffusion at the interface to be the limiting phenomenon regarding the relocalization of the heavy metal

phase. The formation of droplets gives confidence into the coupled Cahn-Hilliard / Navier-Stokes model to reproduce the stratification transitory during IVR. Further simulations should be performed with a lower and more realistic viscosity. It would be interesting to perform additional computations with smaller values of the interface thickness, which would require a more resolved mesh, to study the convergence of the model. Then, while the model parameters impact on the regime transition were found coherent, the increase of the accumulated volume of iron at the bottom that seems to be due to this regime change **remains** not clearly explained. In any case, the limits of the pseudo-binary modeling have been reached and further quantitative simulations should be performed considering a pseudo-ternary thermodynamics model or, even better, a quaternary one.

## Acknowledgments

This work was supported by the CEA (Commissariat à l'énergie atomique et aux énergies alternatives) and EDF (Electricité de France). The computations were performed on the clusters of Ecole Polytechnique and GENCI-IDRIS (project 0042B07727). **The collaboration between PMC and the Wigner Research Center was made possible by the CNRS PICS program.**

## References

- [1] T. G. Theofanous, C. Liu, S. Addition, S. Angelini, O. Kymäläinen, and T. Salimassi. In-vessel coolability and retention of a core melt. *Nucl. Eng. Des.*, 169:1–48, 1997.
- [2] O. Kymäläinen, H. Tuomisto, and T. G. Theofanous. In-vessel retention of corium at the Loviisa plant. *Nucl. Eng. Des.*, 169:109–130, 1997.
- [3] M. Fischer, P. Levi, G. Langrock, A. A. Sulatsky, and E. V. Krushinov. The impact of thermal chemical phenomena on the heat fluxes into the RPV during in-vessel melt retention. In *International Congress on Advances in NPPs (ICAPP) 2011*, Nice, France, 2011.
- [4] M. Fukasawa, S. Hayakawa, and M. Saito. Thermal-hydraulic analysis for inversely stratified molten corium in lower vessel. *Journal of Nuclear Science and Technology*, 45(9):873–888, 2008.
- [5] C. Le Guennic, L. Saas, R. Le Tellier, Y. Wu, M. Guingo, and J. Laviéville. Contribution of CFD studies to IVR assessment. In *8th European Review Meeting on Severe Accident Research - ERMSAR-2017*, Warsaw, Poland, 2017.
- [6] D. F. Tsurikov, V. F. Strizhov, S. V. Bechta, V. N. Zagriazkin, and N. P. Kiselev. Main Results of the MASCA1 and 2 Projects. Technical report, Kurchatov Institute, jun. 2007.
- [7] R. Le Tellier, L. Saas, and S. Bajard. Transient stratification modelling of a corium pool in a LWR vessel lower head. *Nucl. Eng. Des.*, 287:68–77, 2015.
- [8] F. Fichot, L. Carénini, N. Bakouta, H. Esmaili, L. Humphries, T. Laato, R. Le Tellier, L. Saas, I. Melnikov, P. Pandazis, S. Weber, R. J. Park, A. Philippov, and V. Strizhov. Elaboration of a phenomena identification ranking table (PIRT) for the modelling of in-vessel retention. *Ann. Nucl. Energy*, 146:107617, 2020.
- [9] L. Carénini, F. Fichot, N. Bakouta, A. Filippov, R. Le Tellier, L. Viot, I. Melnikov, and P. Pandazis. Main outcomes from the IVR code benchmark performed in the IVMR project. *Ann. Nucl. Energy*, 146:107612, 2020.
- [10] A. Shams, D. Dovizio, K. Zwijsen, C. Le Guennic, L. Saas, R. Le Tellier, M. Peybernes, B. Bigot, E. Skrzypek, M. Skrzypek, L. Vyskocil, L. Carenini, and F. Fichot. Status of computational fluid dynamics for in-vessel retention: Challenges and achievements. *Ann. Nucl. Energy*, 135:107004, 2020.

- [11] Luteng Zhang, Yukun Zhou, Simin Luo, Yapei Zhang, G.H. Su, Zaiyong Ma, and Liangming Pan. Large eddy simulation for the thermal behavior of one-layer and two-layer corium pool configurations in HPR1000 reactor. *Applied Thermal Eng.*, 145:38 – 47, 2018.
- [12] C. Cardon. *Modélisation de la diffusion multi-composants dans un bain de corium diphasique oxyde-métal par une méthode d'interface diffuse*. PhD thesis, Ecole polytechnique, 2016. <https://tel.archives-ouvertes.fr/tel-01495502v1>.
- [13] N. Moelens, B. Blanpain, and P. Wollants. An introduction to phase-field modeling of microstructure evolution. *Computer Coupling of Phase Diagrams and Thermochemistry*, 32:268–294, 2008.
- [14] M. Plapp. Phase-Field Modelling of Solidification Microstructures. *Journal of the Indian Institute of Science*, 96(3):179–198, 2016.
- [15] H. Henry and G. Tegze. Self-similarity and coarsening rate of a convecting bicontinuous phase separating mixture: Effect of the viscosity contrast. *Phys. Rev. F*, 3(074306):1–9, 2018.
- [16] A. Celani, A. Mazzino, P. Muratore-Ginanneschi, and L. Vozella. Phase-field model for the Rayleigh–Taylor instability of immiscible fluids. *J. Fluid Mech.*, 622:115–134, 2009.
- [17] H. L. Lukas, S. G. Fries, and B. Sundman. *Computational Thermodynamics: The CALPHAD Method*. Cambridge University Press, Cambridge, New York, 2007.
- [18] L. Carénini, F. Fichot, and N. Seignour. Modelling issues related to molten pool behaviour in case of In-Vessel Retention strategy. *Ann. Nucl. Energy*, 118:363–374, 2018.
- [19] C. Cardon, R. Le Tellier, and M. Plapp. Modelling of liquid phase segregation in the Uranium–Oxygen binary system. *CALPHAD: Computer Coupling of Phase Diagrams and Thermochemistry*, 52:47–56, 2016.
- [20] R. Zanella, G. Tegze, M. Plapp, R. Le Tellier, and H. Henry. Numerical simulation of droplet formation by Rayleigh–Taylor instability in multiphase corium. *Proc. International Topical Meeting on Advances in Thermal Hydraulics (ATH) 2020*, To be published.
- [21] B. Cheynet, P. Chevalier, and E. Fischer. Thermosuite. *Calphad*, 26(2):167–174, 2002.
- [22] R. Le Tellier, L. Saas, and F. Payot. Phenomenological analyses of corium propagation in LWRs: the PROCOR software platform. In *7th European Review Meeting on Severe Accident Research - ERMSAR-2015*, Marseille, France, 2015.
- [23] J. W. Cahn and J. E. Hilliard. Free Energy of a Nonuniform System. I. Interfacial Free Energy. *J. Chem. Phys.*, 28(2):258–267, 1958.
- [24] L. A. Girifalco and R. J. Good. A Theory for the Estimation of Surface and Interfacial Energies. I. Derivation and Application to Interfacial Tension. *J. Phys. Chem.*, 61(7):904–909, 1957.
- [25] International Atomic Energy Agency. Thermophysical Properties of Materials for Nuclear Engineering: A Tutorial and Collection of Data. Technical report, nov. 2008. Printed by the IAEA in Austria.
- [26] J. W. Cahn. Phase Separation by Spinodal Decomposition in Isotropic Systems. *J. Chem. Phys.*, 42(1):93–99, 1965.
- [27] R. Zanella, G. Tegze, R. Le Tellier, and H. Henry. Two- and three-dimensional simulations of Rayleigh–Taylor instabilities using a coupled Cahn–Hilliard/Navier–Stokes model. *Phys. Fluids*, 32(12):124115, 2020.
- [28] C. Clanet and J. C. Lasheras. Transition from dripping to jetting. *J. Fluid Mech.*, 383:307–326, 1999.
- [29] D. F. Zhang and H. A. Stone. Drop formation in viscous flows at a vertical capillary tube. *Phys. Fluids*, 9(8):2234–2243, 1997.

- [30] R. Menikoff, R. C. Mjolsness, D. H. Sharp, and C. Zemach. Unstable normal mode for Rayleigh–Taylor instability in viscous fluids. *Phys. Fluids*, 20(12):2000–2004, 1977.
- [31] W. V. Ohnesorge. Die Bildung von Tropfen an Düsen und die Auflösung flüssiger Strahlen. *ZAMM - Journal of Applied Mathematics and Mechanics / Zeitschrift für Angewandte Mathematik und Mechanik*, 16(6):355–358, 1936.